Comparative performance of time-invariant, long-range and short-range forecasting models on the earthquake catalogue of Greece

R. Console,[1] D. A. Rhoades,[2] M. Murru,[1] F. F. Evison,[3,4] E. E. Papadimitriou,[5] and V. G. Karakostas[5]

Received 20 October 2005; revised 3 May 2006; accepted 18 May 2006; published 13 September 2006.

[1] Time-invariant, long-range, and short-range forecasting models were fitted to the earthquake catalogue of Greece for magnitudes 4.0 and greater to optimize their ability to forecast events of magnitude 6.0 and greater in the period 1966–1980. The models considered were stationary spatially uniform and spatially varying Poisson models, a long-range forecasting model based on the precursory scale increase phenomenon with every earthquake regarded as a precursor according to scale, and epidemic type short-range forecasting models with spatially uniform and spatially varying spontaneous seismicity. Each of the models was then applied to the catalogue for 1981–2002, and their forecasting performance was compared using the log likelihood statistic. The long-range forecasting model performed substantially better than the time-invariant models, and the short-range forecasting models performed substantially better again. The results show that the information value to be gained from modeling temporal and spatial variation of earthquake occurrence rate, at both long and short range, is much greater than can be gained from modeling spatial variation alone.

Citation: Console, R., D. A. Rhoades, M. Murru, F. F. Evison, E. E. Papadimitriou, and V. G. Karakostas (2006), Comparative performance of time-invariant, long-range and short-range forecasting models on the earthquake catalogue of Greece, *J. Geophys. Res.*, *111*, B09304, doi:10.1029/2005JB004113.

1. Introduction: Earthquake Forecast and Its Verification

[2] A variety of approaches have been applied to the forecasting of earthquakes. Some are based on empirical observations of precursory phenomena, others on physical modeling of the earthquake process, and a third class on statistical analysis of patterns of seismicity.

[3] Regarding the third class, there is growing interest in the use of space-time point process models to describe regional earthquake occurrence. In such models, the earthquake catalogue for a region is regarded as the realization of a point process described usually by a generalized Poisson distribution with each event characterized by its location-time-magnitude coordinates (x, y, t, m), and the process as a whole is defined by a limited number of free parameters. Specification of the parameters allows the computation of the earthquake occurrence rate density on a continuous space-time-magnitude domain. This formulation allows the estimate of the likelihood function of an earthquake catalogue, and the assessment of the maximum likelihood (ML) parameters of the model. Another possibility given by such formulation is the computation of the likelihood ratio (performance factor) of two models based on a given catalogue, as a measure of their relative information value, with one model considered as a null hypothesis [*Rhoades and Evison*, 1979, 1989; *Evison and Rhoades*, 1997; *Kagan and Jackson*, 2000]. This allows a systematic approach to improvement of the models through formal testing of the value of proposed refinements. Such an approach is now being applied in regional earthquake likelihood model (RELM) testing in southern California (D. Schorlemmer and M. C. Gerstenberger, RELM Testing Center, submitted to *Seismological Research Letters*, 2005; D. Schorlemmer et al., Earthquake likelihood model testing, submitted to *Seismological Research Letters*, 2005; R. Console et al., Real time forecasts through an earthquake clustering model constrained by the rate-and-state constitutive law: Comparison with a purely stochastic ETAS model, submitted to *Seismological Research Letters*, 2005).

[4] Progress is being made with developing the Epidemic Type Aftershock Sequence (ETAS) branching model of seismicity that offers a quantification of earthquake interactions. The ETAS model has been used in many studies to describe or predict the spatiotemporal distribution of seismicity and reproduces many properties of real seismicity (see *Ogata* [1998], *Console and Murru* [2001], *Console et al.* [2003], and *Helmstetter and Sornette* [2002, 2003] for

[1] Istituto Nazionale di Geofisica e Vulcanologia, Rome, Italy.
[2] Institute of Geological and Nuclear Sciences, Lower Hutt, New Zealand.
[3] Institute of Geophysics, School of Earth Sciences, Victoria University of Wellington, Wellington, New Zealand.
[4] Deceased 25 January 2005.
[5] Geophysics Department, University of Thessaloniki, Thessaloniki, Greece.

0148-0227/06/2005JB004113$09.00

reviews). In this model the clustering of earthquakes is described by a process in which every earthquake is a main shock with its own aftershock sequence decaying according to the modified Omori law, and with magnitude distribution following the Gutenberg-Richter law. Although the decay in time, described by the Omori law, may have temporal variations up to very large timescales, this model is conventionally considered to be a short-range forecasting model because the temporal variation of an earthquake's contribution to the subsequent seismicity rate is greatest immediately after the earthquake occurs.

[5] *Console and Murru* [2001] and *Console et al.* [2003] showed that a simple clustering model of the ETAS type exhibits a much higher likelihood than the time-invariant Poisson hypothesis. Most of the information value of such models derives from their ability to forecast small aftershocks. Here we examine their ability to forecast the largest earthquakes in a catalogue.

[6] Progress is also being made with long-term forecasting models based on patterns of seismicity that evolve on a timescale of a few years to a few decades. Of principal interest here is a model based on the precursory scale increase phenomenon [*Evison and Rhoades*, 2001, 2004] and the associated predictive scaling relations. *Rhoades and Evison* [2004, 2005] fitted such an EEPAS (Every Earthquake a Precursor According to Scale) forecasting model, to the New Zealand earthquake catalogue, and subsequently applied it, with most parameters unchanged, to recent periods of the catalogues of California and Japan. In both cases it was shown to be more informative than a baseline Poisson model fitted to earlier periods of the same catalogues. It has also been fitted at lower magnitudes to the National Research Institute for Earth Sciences and Disaster Prevention (NIED) catalogue of the Kanto region, central Japan, with similar results [*Rhoades and Evison*, 2006]

[7] Although the ETAS and EEPAS models are numerically different, it is intriguing to speculate that they might both be linked to the physical process of earthquake triggering by coseismic stress changes. In this regard, it has been shown that earthquake triggering (e.g., ETAS, rate-and-state friction) models are sufficient to explain some general features of the precursory scale increase phenomenon, i.e., an increase in the number and average magnitude of earthquakes before a main shock [*Helmstetter et al.*, 2003]. However, the same models have not been shown to offer any specific explanation of the associated predictive scaling relations.

[8] A number of methods dealing with precursory seismicity changes that are not applied in this study have already been published in the seismological literature during the last few decades. For instance, a series of numerical algorithms to make intermediate term earthquake predictions have been developed by a Russian group under the direction of V. I. Keilis-Borok using pattern recognition techniques [*Keilis-Borok*, 1990, 1996]. Belonging to this series, the *M*8 intermediate-term earthquake prediction algorithm was designed by retroactive analysis of dynamics of seismic activity preceding the greatest, magnitude 8.0 or more, earthquakes worldwide, hence its name [*Keilis-Borok and Kossobokov*, 1987].

[9] More recently a group of researchers have applied a new approach to earthquake forecasting based on a Pattern Informatics (PI) method to various zones of the world like California and Japan [*Chen et al.*, 2006; *Holliday et al.*, 2005; K. Z. Nanjo et al., Pattern informatics and its application for optimal forecasting of large earthquake in Japan, submitted *Pure Applied Geophysics*, 2005]. This technique can be used to detect precursory seismic activation or quiescence and make earthquake forecasts. It quantifies temporal variations in seismicity patterns with the objective to reduce the areas of earthquake risk relative to those given by long-term hazard assessments.

[10] Every forecast hypothesis needs a robust statistical validation, to be carried out on data sets that are different from those used for their set up [*Console*, 2001]. This statistical validation should take into account not only the number of successes, but also the rate of false alarms and missed alarms produced by the method under analysis. The concept of probability gain [*Aki*, 1981, 1989] has received a considerable credit for this purpose. The retrospective and forward validation of the M8 and other methods developed by the same above mentioned group is mainly based on this concept.

[11] Another forecast verification procedure is based on the Relative Operating Characteristic (ROC) diagram that has been long used for forecast verification in the atmospheric sciences (e.g., in binary forecasting of tornadoes, El Niños) The ROC diagram considers the fraction of failures to predict and the fraction of false alarms. *Molchan* [1997] has used a modification of this method to evaluate the success of intermediate term forecasts. The Akaike information criterion (AIC) has also become quite popular among seismologists as a method for comparing two or more forecasting models [see, e.g., *Ogata*, 1998]. This method takes into account the different number of free parameters to be assessed under different hypotheses, and can be used without an independent data set for testing.

[12] In this study we are using the above mentioned performance factor, i.e., the ratio between the likelihood of the same earthquake catalogue under two different hypotheses. Here we want to stress the fact that the concept of likelihood considers the probability density of the events that have actually occurred, as well as the integral of that density over the total spatiotemporal considered [*Console and Lombardi*, 2002]. In this respect the likelihood ratio takes full account of the quantity of alarms, and penalizes models that make this number larger.

2. Time-Invariant Models of Seismicity

[13] Conceptually, the simplest models are time-invariant, and are based on the notion that earthquakes continually recur on the same sources. Time-invariant models are widely used in probabilistic seismic hazard analysis as a basis for engineering design of structures, where the time frame of interest is the expected life of the structure, usually from a few decades to a few centuries. In practice, the models are complex because of the incorporation of several different kinds of data, including instrumental, historical and paleoseismicity, rates of fault slip and Earth deformation patterns, and subjective judgments of various kinds. The long time frame of interest and the model complexity have put barriers in the way of systematic testing, so that the information value of many recent refinements is unknown.

In contrast, the simple time-invariant models considered here are derived solely from the earthquakes in the instrumental catalogue.

[14] Time-invariant models of seismicity play two roles in this study. First, they are needed as reference models against which time-varying models can be compared. Second, they are used as models of the spontaneous component of seismicity (i.e., to initiate new clusters) within short-term clustering models. We consider two different time-invariant models, which are both forms of a stationary Poisson model. These are the spatially uniform Poisson (SUP) and spatially varying Poisson (SVP) models. The former model has value mainly as a model of least information.

[15] For the magnitude distribution of both models, we assume the validity of the Gutenberg-Richter law:

$$\mu(x,y,m) = \mu_o(x,y)\beta e^{-\beta(m-m_o)}, \quad (1)$$

where $\mu(x, y, m)$ is the space density of earthquakes of magnitude equal to or larger than m; $\mu_o(x, y) = \mu(x, y, m_o)$ is the space density of earthquakes of magnitude equal to or larger than m_o; β is a characteristic parameter of each seismogenic area, supposed to be approximately independent of time and of the space coordinates; β is linked to the well-known b parameter by the relationship $\beta = b \ln(10)$.

[16] The space-magnitude density of earthquakes is

$$\lambda_o(x,y,m) = \mu_o(x,y)e^{-\beta(m-mo)}. \quad (2)$$

In both equations (1) and (2) the choice of m_o is not critical, provided that the set of data is complete above it.

[17] In the SVP model, we regard the space density $\mu_o(x, y)$ as a continuous, smooth function of the geographical coordinates (x, y). It is obtained by a Gaussian smoothing of the catalog, following the method introduced by *Frankel* [1995] (see Appendix A). In the SUP model the space density is uniform, and hence independent of location (x, y). It is given by the number of events of magnitude above m_0 in each cell divided by the total surface area considered. In both models the catalogue used in the smoothing process is not declustered.

3. Short-Range Forecasting Models Based on Earthquake Clustering

[18] Here we consider the short-term clustering properties of earthquakes and give a brief outline of the method for modeling the interrelation of any earthquake with any other. Though the interaction among earthquakes can be physically justified by the modification in the stress field caused by a dislocation on a fault, this method is based on a purely statistical approach. The details are given by *Ogata* [1998], *Console and Murru* [2001], and *Console et al.* [2003, 2006].

[19] It is widely recognized that the occurrence of a seismic event has influence on the probability of occurrence of future ones. In our clustering models we assume that all previous earthquakes can induce further seismic activity as in the epidemic model (ETAS) introduced by *Ogata* [1989, 1998]. Hence the expected resultant rate density of seismic events, taking into account the influence of the previous inducing earthquakes (x_i, y_i, t_i, m_i: $i = 1, \ldots, N$), can be written as

$$\lambda(x,y,t,m) = f_r\lambda_0(x,y,m) + \sum_{i=1}^{N} H(t-t_i)\lambda_i(x,y,t,m), \quad (3)$$

where f_r is a factor called the "failure rate" (i.e., the ratio between the expected number of independent events and the total number of events), $\lambda_0(x, y, m)$ represents the time-invariant background seismicity expressed as in (2), t_i is the occurrence time of the earthquakes, the total number of which is N, $H(t)$ is the step function, and $\lambda_i(x, y, t, m)$ is the single contribution of the previous earthquakes. The first and the second term on the right hand side of (3) represent the time-invariant "spontaneous" and the time-varying "induced" seismicity, respectively. The rate density corresponding to any earthquake is the sum of these two components. We consider two different versions of (3), in which the spontaneous component $\lambda_0(x, y, m)$ represents either the SUP or SVP model. The corresponding epidemic models are denoted SUP-E and SVP-E, respectively. The form of the induced seismicity component is the same for both models.

[20] We hypothesize that the contribution of any previous earthquake (x_i, y_i, t_i, m_i) to the occurrence rate density of the subsequent earthquakes is decomposable (for $t > t_i$) into three factors, respectively representing the time, space and space magnitude distribution, as

$$\lambda_i(x,y,t,m) = Kh(t-t_i)f(x-x_i,y-y_i)\beta e^{\alpha m_i-\beta m}, \quad (4)$$

where K and α are constant parameters and $h(t)$ and $f(x, y)$ are the time and space densities, respectively.

[21] For the time dependence, we adopt in a general way the modified Omori law [*Ogata*, 1989] that is to be applied to any of the subsequent earthquakes with respect to all the previous ones:

$$h(t) = (t+c)^{-p}, \quad (5)$$

where c and p are characteristic parameters of the process. If $p > 1$, $h(t)$ can be normalized to integrate to 1 by applying the constant factor $(p-1)c^{p-1}$, but if $p \leq 1$, the integral of $h(t)$ is infinite, implying that each earthquake induces an infinite number of subsequent earthquakes, although only a finite number in any finite time interval. Here we do not restrict p to be greater than 1, because we wish to optimize the fit of (5) over small values of t.

[22] We model the spatial distribution of the induced seismicity by a function $f(x - x_i, y - y_i)$ that has circular symmetry around the location (x_i, y_i) of a triggering event of magnitude m_i and is normalized to 1. In polar coordinates,

$$f(r,\theta) = \frac{(q-1)}{\pi}\frac{d^{2(q-1)}}{(r^2+d^2)^q}, \quad (6)$$

where r is the distance from (x, y) to (x_i, y_i) and d is equal to $d_0\ 10^{(m_i-m_0)/2}$ so that the average triggering distance of the aftershock zone is proportional to the square root of the

main shock rupture area, as observed in real data [*Kagan*, 2002]. In this way, d depends on the magnitude of the triggering event. The free parameters d_0 and q control the shape of the distribution.

[23] As to the dependence on the magnitude m_i of the previous earthquakes, we are introducing here a generalization of the *Reasenberg and Jones* [1989] hypothesis (see Appendix B), that is coincident with our algorithm only if $\alpha = \beta$.

[24] The set of parameters has to be adjusted in order to reach the best fit of the respective models to the data. The procedure adopted in this study reflects that used by *Console and Murru* [2001] and *Console et al.* [2003] and previously introduced by *Ogata* [1998]. It consists in searching for the maximum of the log likelihood function of a realization of seismic events described by a catalogue $\{x_j, y_j, t_j, m_j, j = 1, \ldots, N\}$:

$$\ln L = \sum_{j=1}^{N} \ln\left[\lambda(x_j, y_j, t_j, m_j) V_0\right] - \int_X \int_Y \int_T \int_M \lambda(x, y, t, m) \cdot dxdydtdm, \tag{7}$$

where $V_o = \int_X \int_Y \int_T \int_M dxdydtdm$ is a coefficient whose dimensions are equal to those of the inverse of the rate density $\lambda(x_j, y_j, t_j, m_j)$.

4. Long-Range Forecasting Model Based on the Precursory Scale Increase

[25] In the seismicity of well-catalogued regions from a variety of tectonic settings, major shallow earthquakes are usually preceded in the long term by an increase in both the magnitude level and the rate of occurrence of minor earthquakes, in an area not much larger than that later occupied by the epicenters of the major earthquake and its aftershocks. This is the precursory scale increase (Ψ) phenomenon. *Evison and Rhoades* [2004] presented 47 examples of the Ψ phenomenon and from each one of them tabulated the main shock magnitude, M_m, the precursor magnitude M_P (defined as the average magnitude of three largest precursory earthquakes), the precursor time T_P (the time between the onset of Ψ and the main shock) and the area A_P of the region in which the phenomenon was observed. They showed that all of these variables are linked by simple scaling relations, and that M_P is predictive of the magnitude, time and location of the major earthquake through linear regressions of M_m, $\log T_P$ and $\log A_P$ on M_P.

[26] The EEPAS forecasting model, introduced by *Rhoades and Evison* [2004, 2005], is a space-time point process model which adopts the Ψ predictive scaling relations, but sets aside the problem of recognizing the Ψ phenomenon before the major earthquake occurs. It applies the predictive relations to all earthquakes, regarding each as a long-term precursor of larger earthquakes to follow later. The probability of future earthquake occurrence is derived directly from past earthquakes in the catalogue, with every earthquake making a transient contribution, as in the epidemic models described above. The general form of the model is identical to equation (3), but the second term no longer represents induced seismicity. Rather, it quantifies the strength of the evidence that a long-term seismogenic process is taking place for an earthquake at a given time, magnitude and location. The contribution of the ith earthquake to the rate density is

$$\lambda_i(x, y, t, m) = w_i \eta(m_i) f_{1i}(t) g_{1i}(m) h_{1i}(x, y), \tag{8}$$

where w_i is a weighting factor, η is a normalization function to ensure that the forecast is consistent with the Gutenberg-Richter law, and f_{1i}, g_{1i}, and h_{1i} are probability densities for time, magnitude and location, respectively. The time density f_{1i} is lognormal and takes the form

$$f_{1i}(t) = \frac{1}{(t - t_i)\sigma_T \ln(10)\sqrt{2\pi}} \exp\left[-\frac{1}{2}\left(\frac{\log(t - t_i) - a_T - b_T m_i}{\sigma_T}\right)^2\right], \tag{9}$$

where a_T, b_T, and σ_T are parameters. The magnitude density g_{1i} is normal and takes the form

$$g_{1i}(m) = \frac{1}{\sigma_M \sqrt{2\pi}} \exp\left[-\frac{1}{2}\left(\frac{m - a_M - b_M m_i}{\sigma_M}\right)^2\right], \tag{10}$$

where a_M, b_M, and σ_M are parameters. The location density h_{1i} is bivariate normal with circular symmetry and takes the form

$$h_{1i}(x, y) = \frac{1}{2\pi\sigma_A^2 10^{b_A m_i}} \exp\left[-\frac{(x - x_i)^2 + (y - y_i)^2}{2\sigma_A^2 10^{b_A m_i}}\right], \tag{11}$$

where σ_A and b_A are parameters. The normalization function is

$$\eta(m) = \frac{b_M(1 - f_r)}{E(w)} \exp\left[-\beta\left(a_M + (b_M - 1)m + \frac{\sigma_M^2}{2}\right)\right], \tag{12}$$

where β is as in (1) and $E(w)$ is the mean weight of earthquakes in the catalogue, which can be estimated at any time by the average over past earthquakes.

[27] When a magnitude threshold of completeness m_o is applied, an adjustment must be made to compensate for the missing contribution from earthquakes with magnitude below m_o as explained by *Rhoades and Evison* [2004] (see Appendix C).

[28] In previous applications of the model, two different weighting strategies have been applied: a strategy in which all earthquakes are assigned equal weights and one in which aftershocks are down weighted. Only the latter strategy is employed here, because it tends to improve the performance of the model by a small margin. The weights w_i take values in the interval [0,1] and are derived from the rate densities of a quasi-static baseline model, fashioned after a model proposed by *Jackson and Kagan* [1999], and a model incorporating aftershocks, which bears many similarities to the epidemic model described above, but has some intentional differences. These models each have a set of parameters, (a, d, and s) and (p, c, σ_U, ν, κ, and δ), respectively, which must be fixed or estimated before the

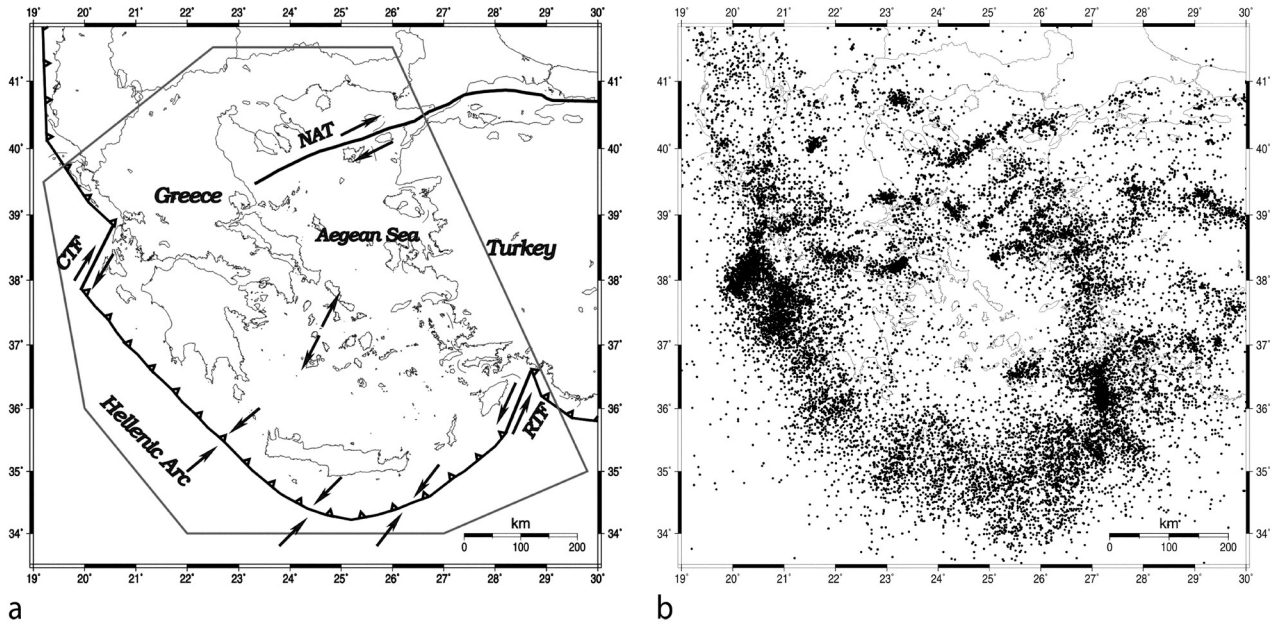

Figure 1. Map of Greece showing (a) the polygonal region of surveillance and main tectonic features and (b) epicenters of earthquakes with $M \geq 4.0$ in the period 1966–2002.

EEPAS model is fitted [*Rhoades and Evison*, 2004]. See Appendix C for details.

5. Application to the Catalogue of Greece

[29] In this study we fit and test the models described above using the non declustered instrumental catalogue of the seismicity of Greece [*Papazachos et al.*, 2005] from 1966 through 2002, focusing on the polygonal region of surveillance shown in Figure 1.

[30] The study area is a well-catalogued seismically active region incorporating a variety of tectonic styles. It belongs to the extensional back-arc Aegean region that includes south Bulgaria and former Yugoslavia, northern and central Greece, southern Aegean volcanic arc, and the southwestern and central western Turkey (Figure 1). The Aegean region is one of the most active tectonic regions of the Alpine-Himalayan belt, with its most prominent tectonic feature the subduction of the eastern Mediterranean lithosphere under the Aegean Sea [*Papazachos and Comninakis*, 1970] along the Hellenic Arc. The seismicity is very high throughout the arc, which is dominated by thrust faulting with a NE-SW direction of the axis of maximum compression. A belt of thrust faulting runs along the southwestern coasts of Yugoslavia and continues south along the coastal regions of Albania and northwestern Greece, resulting from continental collision between Outer Hellenides and the Adriatic microplate. The direction of the maximum compression axis is almost normal to the direction of the Adriatico-Ionian geological Zone. Between continental collision to the north and oceanic subduction to the south, the dextral strike-slip Cephalonia Transform Fault (CTF) is observed [*Scordilis et al.*, 1985] in agreement with the known relative motion of the Aegean and eastern Mediterranean. *McKenzie* [1978] showed that the northward motion of the Arabian plate pushes the smaller Anatolian plate westward along the North Anatolian Fault, continuing along the North Aegean Trough (NAT) region, which is the boundary between the Eurasian and south Aegean plates. Right-lateral strike-slip motion associated with the North Anatolian Fault (NAF) appears to become more distributed in the north Aegean Sea, which is characterized by a combination of right-lateral shear and extension. This motion is transferred into the Aegean but in a southwesterly direction. The long-term seismogenesis of the recent large earthquakes in this region has been discussed by *Papadimitriou et al.* [2006].

[31] The catalogue considered for the analysis (see the polygon in Figure 1) is complete and homogeneous for magnitudes $M \geq 4.0$ from 1966 up to date. Inside the region of surveillance, 16,410 earthquakes are listed in the catalogue for the period analyzed, which we split into two subsets: a learning period from 1966 through 1980 comprising 4476 earthquakes, and a test period from 1981 through 2002 comprising 11,934 earthquakes. To avoid edge effects, the catalogue from 1950 on, including earthquakes outside the region of surveillance but within the latitude range 33.0°–42.5°N and longitude range 18.0°–30.0°E, was used to generate the forecasts for all time-dependent models. Though this early part of the catalogue cannot be considered complete, its inclusion has some effect on the expected rate of the earthquakes especially at the beginning of the analyzed period. In this respect, the completeness of the early part of the catalogue is not a critical issue, because only the events of larger magnitude have a stronger and longer duration. In a similar way, it is important to consider also the events outside the edges of the analyzed area, but close to it, for their possible contribution to the expected rate of earthquakes inside the polygon.

[32] The log linear frequency versus magnitude plot of earthquakes in the learning set deviates markedly from the

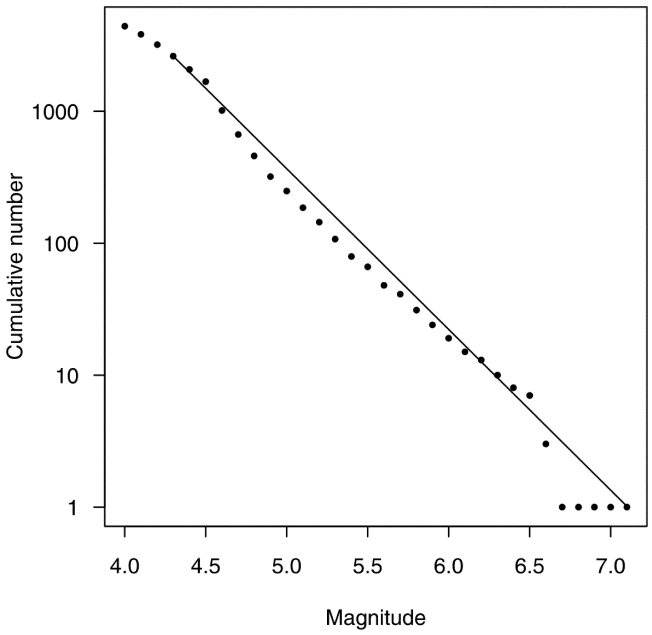

Figure 2. Frequency magnitude relation for earthquakes in the region of surveillance in the learning period 1966–1980. The line shown has slope $b = 1.3$.

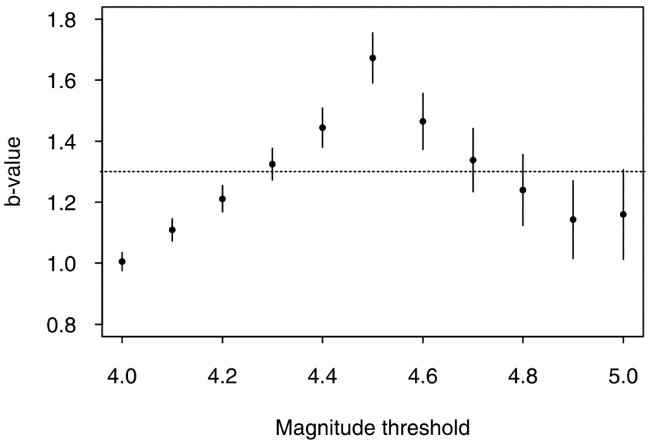

Figure 3. Maximum likelihood estimate of the Gutenberg-Richter b value in the region of surveillance for 1966–1980, and its uncertainty (±2 standard errors), as a function of minimum magnitude threshold.

usual Gutenberg-Richter relation (Figure 2). The observed nonlinearity would be only partially explained by postulating catalogue incompleteness below M 4.5. The maximum likelihood estimate of the b value [*Aki*, 1965] varies significantly with the choice of lower magnitude threshold (Figure 3), and takes values ranging from 1.0 to 1.7, with an average of 1.3, for magnitude thresholds within the range 4.0 to 5.0. The models to be compared all have b value as a parameter, but are sensitive to its value in different magnitude ranges. The time-invariant models depend only on the b value above magnitude 6.0, which is close to 1. The short-range forecasting models are sensitive to the b value across the range of magnitudes, but the larger an earthquake is, the more it contributes to the hazard. The EEPAS model is also sensitive to the b value across the range of magnitudes through the normalization function (equation(12)), but earthquakes in the range $4.0 \leq M \leq 5.0$ contribute most to the rate density for $6.0 \leq M \leq 6.5$. The normalization thus depends on a value that will give a good estimate of the number of earthquakes with $M \geq 6.0$ from the number in the range $4.0 \leq M \leq 5.0$. After all these factors were taken into account, 1.3 was adopted as the b value for the data above M 4.0 as average over all the magnitude range for the time-invariant, short-range and long-range forecasting models.

[33] The time-invariant models, SUP and SVP, were normalized to the total number (19) of earthquakes with $M \geq 4.0$ in the learning set. For the SVP model, the spatial distribution of seismicity $\mu_o(x, y)$ was fitted to the learning period of the catalogue by interpolation from a grid of 100×120 cells, each having a size of 10×10 km, centered on the point 38°N, 24°E. For the short-range forecasting models, SUP-E and SVP-E, we fixed some of the parameters in order to restrict the number of degrees of freedom and get a more robust fit. Specifically, we imposed $q = 1.5$, and $\alpha = \beta$, with $b = 1.3$. The other parameters of the SUP-E and SVP-E models were fitted to the learning set, using maximum likelihood. In order to get a more robust determination of the free parameters, all the earthquakes with $M \geq 4.0$ in the learning set have been considered as target events in the best fit. The fitted values are listed in Table 1.

[34] It is instructive to compare the parameters of the SUP-E and SVP-E models. The value of f_r is lower for SUP-E than for SVP-E, reflecting the lack of spatial information in the time-invariant component. The value of p is lower also, which means that the time distribution of the so-called induced seismicity has a longer tail, perhaps compensating for the lack of spatial information in the time-invariant component.

[35] For the long-range forecasting model, EEPAS, we again fixed some of the parameters in order to get a more robust fit. We imposed $b_M = 1$ (a value which is consistent with perfect scaling of magnitudes and which removes the magnitude dependence from the normalization function η), $b_T = 0.40$, and $b_A = 0.35$. The latter two values are the slopes of regressions of log T_P on M_P and log A_P on M_P, respectively, obtained from 47 examples of the Ψ phenomenon by *Evison and Rhoades* [2004]. We also imposed $f_r = 0$, after checking that this value was close to optimal. In addition, several parameters of the aftershock model used in the determination of the weights w_i were fixed at the values used in previous studies [*Rhoades and Evison*, 2004, 2005]: namely, $c = 0.03$ day, $p = 1.2$, $\sigma_U = 0.0056$, and $\delta = 0.7$. The three parameters of the baseline model (a, d, s) and the remaining two parameters of the aftershock model (ν, κ)

Table 1. Fitted Parameters of the Short-Range Forecasting Models, SUP-E and SVP-E, Optimized Over the Period 1966–1980, and a Threshold Magnitude $m_c = 4.0$

	SUP-E	SVP-E
K, days^{p-1}	0.000642	0.000656
c, days	0.00976	0.0197
p	0.907	1.033
d, km	1.600	1.548
f_r	0.144	0.456

Table 2. Fitted Parameters of the Long-Term Forecasting Model EEPAS and the Associated Baseline and Aftershock Models Optimized Over the Period 1966–1980

EEPAS		Associated Models	
Parameter	Value	Parameter	Value
a_M	1.40	a	0.134
σ_M	0.49	d	9.87
a_T	1.00	s	2.50×10^{-7}
σ_T	0.44	ν	0.421
σ_A	3.34	κ	0.0477

were fitted by maximum likelihood to the learning period. Then, with these parameters all fixed and with $m_c = 6.0$, the free parameters of the EEPAS model were fitted to the learning period, again using maximum likelihood. The fitted parameter values are listed in Table 2.

[36] Comparing the fitted values with those in previous applications of the EEPAS model, a notable feature of Table 3 is the relatively low value of $a_T = 1.0$ (c.f. $a_T = 1.50$ in Table 1 and 1.32 in Table 4 of *Rhoades and Evison* [2005]). If all other parameters were equal, this would indicate a typical precursor time, which is less than half as long as in New Zealand and Japan. However, the value of σ_T here (0.44) is nearly double that used in previous studies (0.23), suggesting a relatively high variability of precursor time within the present region of surveillance. It can probably be attributed to the fact that the strain rates differ significantly between different regions of our study area [*Papazachos and Kiratzi*, 1996], and that the variability of the strain rate is reflected in that of the precursor time.

[37] The aim is to establish the predictive power of the short-range and long-range forecasting models relative to the time-invariant models for earthquakes of significant impact on the population, neglecting the obvious value of the short-range models in forecasting conventional aftershock activity soon after main shocks. Thus we consider the likelihood of the observed earthquakes under the various models taking as target events only the strongest earthquakes. We have arbitrarily selected two different lower magnitude thresholds: $m_c = 6.0$ and $m_c = 6.5$, in each case adopting an upper magnitude threshold of $m_u = 8.0$ (which is substantially larger than 7.5, the greatest magnitude in the catalogue since 1950). The numbers of target earthquakes in the learning set are 19 and 7, respectively. In the testing set the numbers are 24 and 8, respectively.

[38] The likelihood statistics are given in Table 3 where for each model we list the value of $\Delta\ln L/N$, where $\Delta\ln L$ is the difference between the log likelihood of the model in question ($\ln L$), calculated using equation (7), and the log likelihood of the model of least information (SUP model), and N is the number of earthquakes with $M \geq m_c$ in the region of surveillance over the learning time period. The probability gain per earthquake $G = \exp(\Delta\ln L/N)$ is also reported in Table 3, because it has been preferred by the authors of some previous studies [*Helmstetter et al.*, 2006]. In some ways $\Delta\ln L/N$ gives a more meaningful score, because it is additive rather than multiplicative, while G is much more sensitive to very high scores for individual earthquakes.

Table 3. Results of Fitting the Models to the 1966–1980 Data Set

	$m_c = 6.0$ (Number of Target Events 19)		$m_c = 6.5$ (Number of Target Events 7)	
Model	$\Delta\ln L/N$	G	$\Delta\ln L/N$	G
SUP	0.0	1.00	0.0	1.00
SVP	0.47	1.60	0.62	1.86
EEPAS	1.30	3.65	0.61	1.83
SUP-E	1.57	4.81	2.01	7.46
SVP-E	1.73	5.64	2.40	11.02

Table 4. Performance of Models on 1981–2002 Data Set

	$m_c = 6.0$ (Number of Target Events 24)		$m_c = 6.5$ (Number of Target Events 8)	
Model	$\Delta\ln L/N$	G	$\Delta\ln L/N$	G
SUP	0.0	1.00	0.0	1.00
SVP	−0.16	0.85	−0.33	0.72
EEPAS	1.26	3.51	0.98	2.66
SUP-E	1.81	6.11	1.16	3.19
SVP-E	1.71	5.99	1.15	3.16

[39] These statistics are a measure of the information rate per earthquake of each of the models, relative to SUP, although the values may be biased by the fitting of the models to this data set. The values in Table 3 indicate that the information value of the models increases from SUP in the order SVP, EEPAS, SUP-E, SVP-E for $m_c = 6.0$. Thus the spatially varying time-invariant model is more informative than the spatially uniform time-invariant model, the long-range forecasting model is more informative than the time-invariant models, and the short-range forecasting models are more informative still.

[40] To obtain an unbiased evaluation of the information value of the models, we must test them on a new and independent data set [*Console*, 2001]. Here we use the time period 1981–2002 in a quasi-prospective way. In this testing phase, the likelihood of each model is evaluated using the parameters obtained from the learning phase. The results are given in Table 4.

[41] The information rate per earthquake is markedly reduced for the SVP and SVP-E models with $m_c = 6.0$, indicating that the larger earthquakes have a different spatial distribution in the test period than in the learning period. In contrast, the information value of the EEPAS model is similar to the learning period. Table 4 demonstrates that both the long-range and short-range forecasting models have a much higher information value than the time-invariant models. However, the information value of the models now increases in a different order SVP, SUP, EEPAS, SVP-E, SUP-E.

[42] A more detailed analysis of the single contribution of each target event to the information value of the forecasts is shown in Figure 4. Figure 4 shows the evolution of the performance factor, i.e., the likelihood relative to the model SUP, for each of the models SVP, EEPAS, SUP-E and SVP-E over the test period (1981–2002). Each vertical step corresponds to a target event, and the step is positive if the occurrence rate predicted by the model is larger than that predicted by the SUP model (i.e., the model forecasts the event). Conversely, the step is negative if the expected

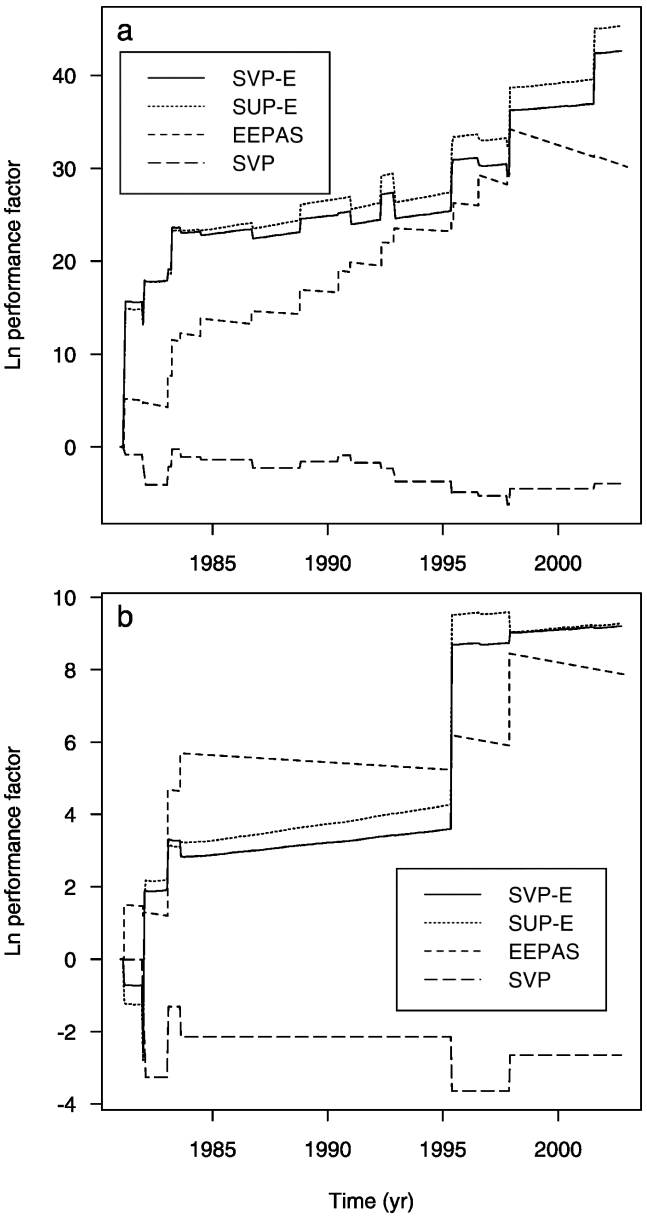

Figure 4. Evolution of the performance factor of the SVP, EEPAS, SUP-E, and SVP-E models with respect to the SUP model computed in steps of 20 days for the test period (1981–2002): (a) for a target magnitude threshold $M_c = 6.0$ and (b) for a target magnitude threshold $M_c = 6.5$.

occurrence rate for the clustering model is smaller than that of the Poisson model (i.e., the model fails to forecast the event). The line segment between any two consecutive steps describes the trend of the performance factor in the nonoccurrence time periods. Its slope is positive if the occurrence rate predicted by the model is smaller than that predicted by the SUP model, and vice versa.

[43] As seen in Figure 4, the large performance factor of the short-range forecasting models is mainly due to a limited number of earthquakes that occurred as part of a cluster, i.e., they occurred in the influence space time volume of previous events. For the target magnitude threshold $M_m = 6.5$ this circumstance occurred only twice of a total of 8 events. For the target magnitude threshold

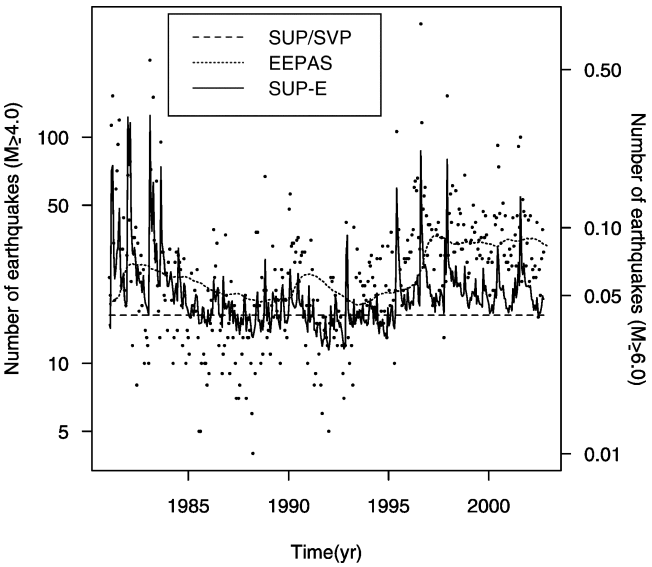

Figure 5. Observed rate of earthquake occurrence (number of earthquakes per 20 day period) for $M \geq 4$ (points) compared with expected rates of occurrence under the models SUP/SVP, EEPAS ($M \geq 6$), and SUP-E for the test period 1981–2002 (lines). Only the left-hand ordinate scale applies to the observed numbers, and only the right-hand scale applies to the EEPAS model. Both ordinate scales apply to the other models.

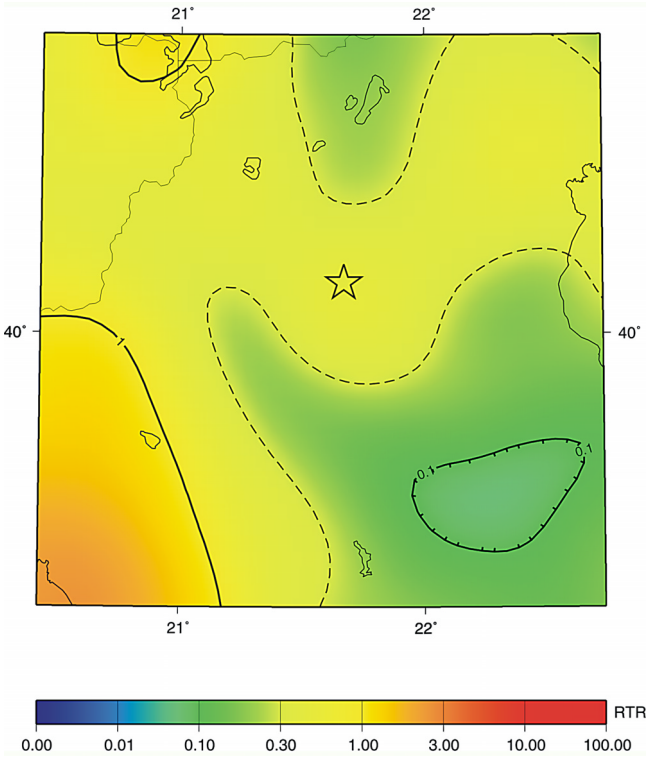

Figure 6. Average rate of earthquake occurrence for $M > 6.35$ over the year 1995 under the EEPAS model, using data up to the end of 1994. The rate is expressed relative to a reference scale (RTR) in which there is an expectation of 1 earthquake per year exceeding any magnitude m in an area of 10^m km^2. The star marks the epicenter of the M6.6 earthquake of 13 May 1995, 0847:17.0 UT.

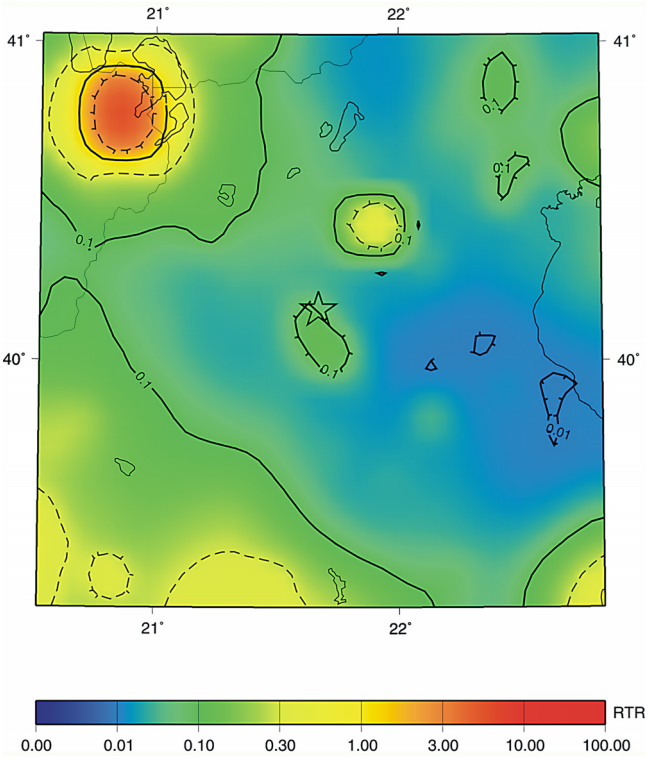

Figure 7. Instantaneous rate of earthquake occurrence (RTR) for $M > 6.35$ at 0840 UT on 13 May 1995 under the SVP-E model. The star marks the epicenter of the $M6.6$ Kozani earthquake of 13 May 1995, 0847:17.0 UT. See Figure 6 caption for definition of RTR scale.

$M_m = 6.0$, 8 events of a total of 24 exhibited a performance factor larger than 10. In some cases a high performance factor arose because of the large expected rate density for earthquakes with $M \geq 6.0$ which themselves can be considered aftershocks of larger earthquakes. This was the case for two clusters which occurred in 1981 and for another in 1983. In the first cluster, the $M6.4$ event of 25 February 1981, with coordinates 38.14°N, 23.09°E, was preceded the previous day by a stronger $M6.7$ event, and followed 9 days later by another $M6.3$ event. In the same year, the $M6.5$ event of 27 December 1981, with coordinates 38.81°N, 24.94°E was preceded 8 days earlier by its $M7.2$ main shock. Finally, the $M6.2$ event of 23 March 1983, which occurred on the Cephalonia fault segment, was the strongest aftershock of the $M7.0$ main shock of 17 January 1983. In other cases a high performance factor arose because of the occurrence of small foreshocks which occurred just prior to an earthquake with $M \geq 6.0$.

[44] In contrast, the high value of the performance factor for the long-range forecasting model is the result of a larger number of relatively small gains. For a majority of earthquakes with $M \geq 6.0$, the performance factor is greater than 1, but there are no really large performance factors for individual earthquakes, such as are seen for the short-range forecasting models.

[45] For a better understanding of the difference between the various models we compare the observed rate of $M \geq 4.0$ events with expected rates of earthquake occurrence under each model, as a function of time (Figure 5). The expected rate is constant for the SUP and SVP models, slowly varying for the EEPAS model, and rapidly varying for the SUP-E and SVP-E models. The rate for the SVP-E model is not shown in Figure 5 but is very similar to that for SUP-E. The observed rate is more variable than any of the modeled rates.

6. Examples of Forecasts Pertaining to Particular Earthquakes

[46] The rate of earthquake occurrence ($M > 6.35$) under the long-range and short-range forecasting models is illustrated for particular times and subsets of the region of surveillance in Figures 6–10. For easy comparison, the rates are expressed relative to a reference (RTR) scale in which there is an expectation of one earthquake per year exceeding any given magnitude m in an area of 10^m km^2. Figures 6–8 refer to a region surrounding the epicenter of the $M6.6$ Kozani earthquake of 13 May 1995 at 0847:17.0 UT. The EEPAS forecast, based on the catalogue up to the end of 2004 and averaged over the whole of the year 1995, is shown in Figure 6. Figures 7 and 8 show the rate of occurrence under the SVP-E model at two instants of time 7 min apart, 0840 and 0847 UT, respectively. The Kozani main shock occurred 17 s after 8.47 am. As Figure 6 shows, the average rate of occurrence under the EEPAS model for 1995 was about 0.5 RTR, and for this magnitude range, there would be little variation of the EEPAS model forecast over a time period as short as 1 year. The instantaneous rate under the SVP-E model at 0840 on 13 May

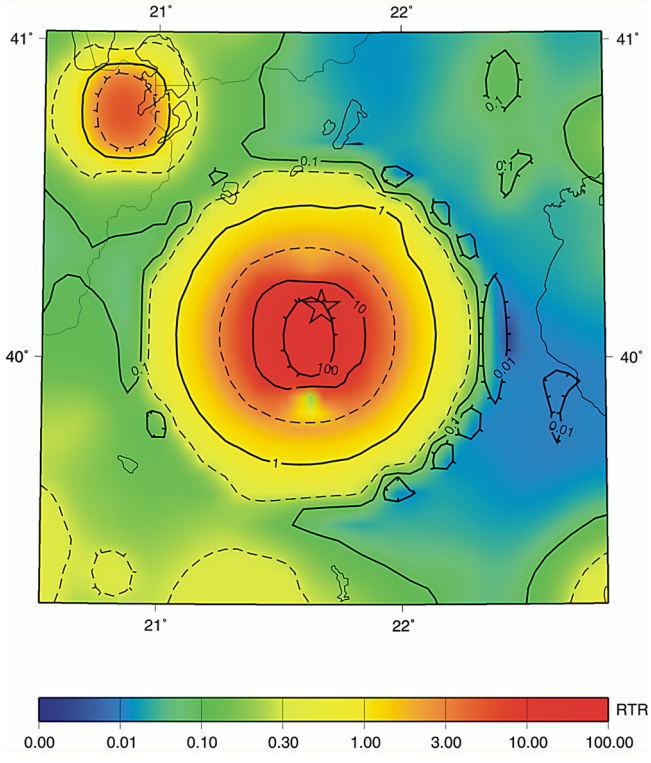

Figure 8. Instantaneous rate of earthquake occurrence (RTR) for $M > 6.35$ at 0847 UT on 13 May 1995 under the SVP-E model. The star marks the epicenter of the $M6.6$ Kozani earthquake which occurred 17 s later. See Figure 6 caption for definition of RTR scale.

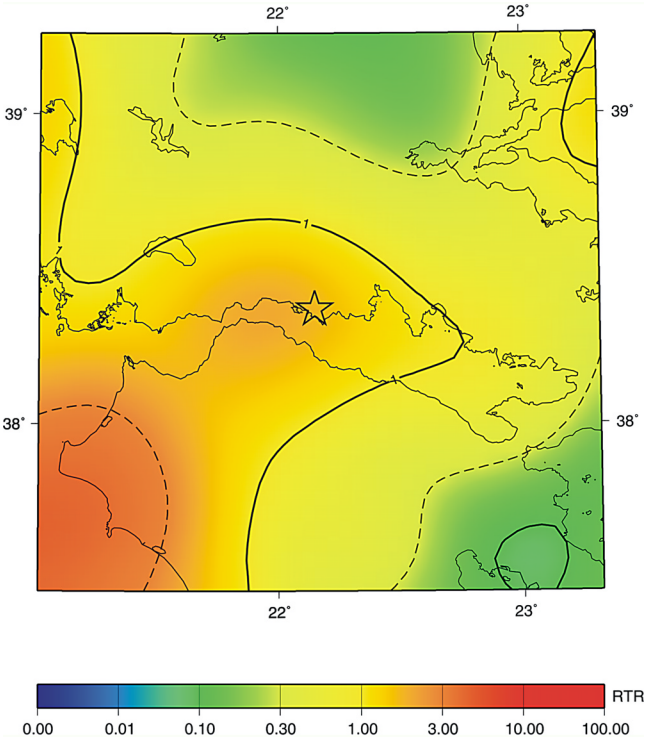

Figure 9. Average rate of earthquake occurrence (RTR) for $M > 6.35$ over the year 1995 under the EEPAS model, using data up to the end of 1994. The star marks the epicenter of the $M6.4$ Aigion earthquake of 15 June 1995 at 0015:49.0 UT. See Figure 6 caption for definition of RTR scale.

1995 was about 0.1 RTR (Figure 7), with no recent earthquakes in the vicinity contributing to the epidemic component of the model. However, following the occurrence of a foreshock of magnitude 4.5 at 0843 UT, the rate was raised to about 100 RTR (Figure 8), which gave a large boost to the performance of the SVP-E model. The proximity of the foreshock to the main shock, in both time and location, caused the short-range forecasts of both the SVP-E and SUP-E models to be far superior to the long-range forecast of the EEPAS model. However, a foreshock occurring so close in time (4 min before) would hardly be useful for a real-time forecast, for two reasons. First, it is not generally practicable to produce a short-range forecast within such a short time interval, and second, every small earthquake in the catalogue, whether a foreshock or not, would in principle have a similar short-term impact on the estimated rate of occurrence.

[47] Another major earthquake in 1995 was the $M6.4$ Aigion earthquake of 15 June 1995. The EEPAS model forecast for 1995 in the vicinity of the epicenter of this earthquake is shown in Figure 9. As Figure 9 shows, the EEPAS model gave an average rate of about 3 RTR for 1995 at the epicenter. Figure 10 shows the instantaneous SVP-E model forecast just before the occurrence of the Aigion main shock at 0015:49.0 UT on 15 June 1995. On this occasion, no foreshock occurred sufficiently close to the time and location of the main shock to boost the rate to a high value. As Figure 10 shows, the rate under the SVP-E model was about 0.5 RTR. The long-range forecast provided by the EEPAS model was therefore more informative for this event than the short-range forecast.

7. Conclusion

[48] These present tests of the relative performance of time-invariant, long-range and short-range forecasting models illustrate that the preparation of a major earthquake is often signaled by precursory changes in the patterns of earthquake occurrence in time, space and magnitude. Even though the precursory signals are noisy, they are strong enough so that both long-range and short-range time-varying estimates of earthquake occurrence are far superior to time-invariant estimates. It is likely that the time-varying estimates will provide opportunities for improved planning of countermeasures against earthquakes on various timescales.

[49] The present study points to opportunities for future research aimed at improving the long-range and short-range forecasting models. Two immediate prospects are evident. First, short-range forecasting could perhaps be improved by adopting a long-range forecasting model, rather than a time-invariant model, for the spontaneous component of seismicity. Second, long-range forecasting could perhaps be improved by allowing for the fact that any forecasted earthquake is likely to have its own aftershocks, and that some of the aftershocks may be above the magnitude threshold that is of interest. Finally, the likelihood-based approach adopted here and elsewhere allows a systematic approach to improved forecasting by the formal testing of

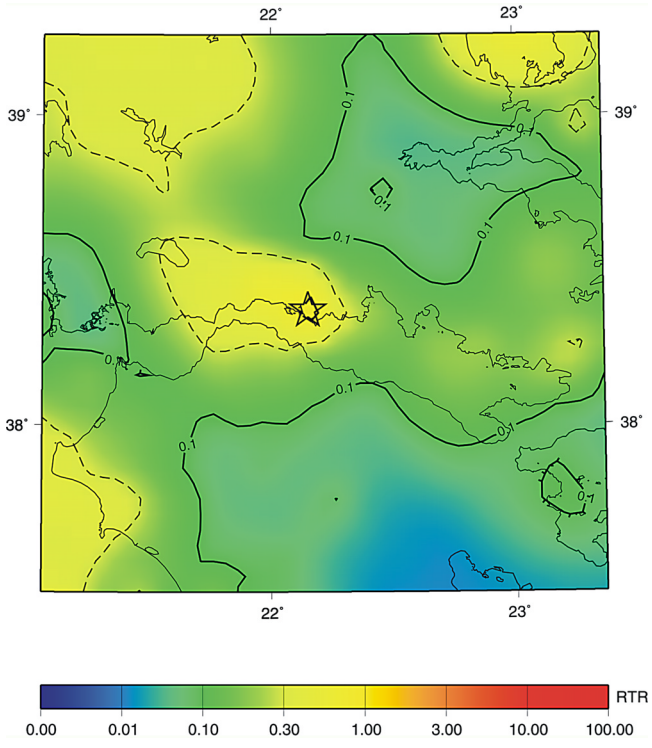

Figure 10. Instantaneous rate of earthquake occurrence (RTR) for $M > 6.35$ at 0015 UT on 15 June 1995 under the SVP-E model. The star marks the epicenter of the $M6.4$ Aigion earthquake which occurred 49 s later. See Figure 6 caption for definition of RTR scale.

proposed model refinements, and may lead, in the long run, to much improved forecasting models on a variety of timescales, that make use not only of earthquake catalogue data, but of other related geophysical data and modeling.

Appendix A: Smoothing in the SVP Model

[50] In the SVP model, the smoothing algorithm introduced by *Frankel* [1995] is adopted. First, the region to be analyzed is subdivided into square cells of appropriate size. The number of earthquakes N_k in cell k represents the maximum likelihood estimate of N_0 for that cell (for earthquakes above m_0). The grid of N_k values is spatially smoothed by multiplying these values by a Gaussian function with correlation distance d. For each cell k, the smoothed value N_k is obtained from

$$\tilde{N}_k = \frac{\sum_l N_k \exp\left(-\Delta_{kl}^2/d^2\right)}{\sum_l \exp\left(-\Delta_{kl}^2/d^2\right)},$$

where Δ_{kl} is the distance between the centers of the kth and lth cells. In equation (6), N_k is normalized to preserve the total number of events. The optimal parameter d for the Gaussian function is obtained by means of the criterion outlined by *Console and Murru* [2001]. It consists of a trial and error search for the maximum likelihood of a subcatalogue containing about half of the total number of events, under the model obtained from the other half.

[51] The values of N_k obtained so far still change abruptly from one cell to another. In order to obtain a continuous function, the single value of $\mu_0(x, y)$ is computed by interpolation between the four cells whose centers surround the point (x, y). The result is given as number of events per cell size, in the total time spanned by the catalog. In order to have it in units of number of events per unit time and per unit area, it must be divided by the total time of the input catalog and the area of a cell.

Appendix B: Number of Aftershocks

[52] *Reasenberg and Jones* [1989] (RJ) analyzed numerous aftershock sequences in California. They counted the number of aftershocks which occurred after main shocks within suitably defined space and time volumes of influence. Their analysis leads to the conclusion that the number N of aftershocks so defined depends on the main shock magnitude through

$$N = N_0 10^{b(m-m_0)},$$

where N_0 is a parameter characterizing the productivity of a given sequence, b is the slope of the Gutenberg-Richter frequency-magnitude distribution, m is the main shock magnitude, and m_0 is the completeness magnitude above which the aftershocks are catalogued.

[53] The main physical implication of the RJ model is that for $b = 1$ the number of aftershocks is proportional to size of the fault area, if we assume that the log of the fault area and the log of the seismic moment scale with m and $1.5m$, respectively.

[54] The importance of this model consists in the presence of the b parameter in the exponential modeling the aftershock production. So, as the same b parameter appears with a minus sign also in the frequency-magnitude distribution, it follows that the total number of aftershocks produced by all the main shocks of a given magnitude class is the same as that produced by a magnitude class smaller or larger by one unit.

Appendix C: Adjustment and Weighting in the EEPAS Model

[55] An adjustment to the EEPAS rate density is necessary when a lower magnitude threshold m_0 is applied to the precursory earthquakes. To compensate for the missing contribution from earthquakes below magnitude m_0, the estimated rate density $\lambda(t, m, x, y)$ should be inflated by a factor of $1/\Delta(\mathrm{m})$, given by

$$\Delta(m) = \Phi\left(\frac{m - a_M - b_M m_0 - \sigma_M^2 \beta}{\sigma_M}\right), \tag{C1}$$

where Φ is the standard normal integral.

[56] Weights in the EEPAS model are computed using a quasi-static baseline model and an aftershock model [*Rhoades and Evison*, 2004]. In the baseline model, which is fashioned after a model proposed by *Jackson and Kagan* [1999], the rate density λ_0 depends on Proximity to Past Earthquakes (PPE) in the catalogue. The PPE model has the form

$$\lambda_0(t, m, x, y) = f_0(t) g_0(m) h_0(x, y), \tag{C2}$$

where f_0 is the time function, g_0 is the magnitude density and h_0 is the density for location. The time function is given by

$$f_0(t) = \frac{1}{t - t_0}. \tag{C3}$$

The magnitude density is that implied by the Gutenberg-Richter frequency-magnitude law:

$$g_0(m) = \beta \exp[-\beta(m - m_c)], \tag{C4}$$

where β is defined as in equation (1). Finally, the function h_0 is the sum, over all earthquakes from time t_0 up to, but not including, time t, of smoothing kernels of the form

$$h_{0i}(r_i) = a(m_i - m_c)\frac{1}{\pi}\left(\frac{1}{d^2 + r_i^2}\right) + s, \tag{C5}$$

where r_i is the distance in km between (x, y) and the epicenter (x_i, y_i) of the ith earthquake; a is a normalization constant; d is a smoothing distance; and s is a small constant to allow for earthquakes far from past earthquakes.

[57] The aftershock model (with rate density λ') is of the form

$$\lambda'(t, m, x, y) = \nu\lambda_0(t, m, x, y) + \kappa \sum_{t_i \geq t_0} \lambda_i'(t, m, x, y), \tag{C6}$$

where λ_0 is as above; ν is the proportion of earthquakes that are not aftershocks; κ is a normalization constant; and λ'_i takes the form

$$\lambda'_i(t,m,x,y) = f_{2i}(t)g_{2i}(m)h_{2i}(x,y). \quad \text{(C7)}$$

Here, f_{2i}, g_{2i} and h_{2i} are functions for time, magnitude and location of the aftershocks of the ith earthquake. The time distribution follows the modified Omori law, i.e.,

$$f_{2i}(t) = H(t-t_i)\frac{p-1}{(t-t_i+c)^p}, \quad \text{(C8)}$$

where t_i is the time of the ith earthquake and c and p are parameters with $c > 0$ and $p > 1$. The magnitude distribution follows the Gutenberg-Richter law, with the stipulation that the magnitude of an aftershock is smaller than that of its main shock by at least δ units, i.e.,

$$g_{2i}(m) = H(m_i - \delta - m)\beta \exp[-\beta(m-m_i)]. \quad \text{(C9)}$$

Note that g_{2i} is not a probability density in that it does not integrate to 1. The spatial distribution of aftershocks is given by

$$h_{2i}(x,y) = \frac{1}{2\pi\sigma_U^2 10^{m_i}} \exp\left[-\frac{(x-x_i)^2+(y-y_i)^2}{2\sigma_U^2 10^{m_i}}\right], \quad \text{(C10)}$$

where σ_U is a constant parameter.

[58] To assign a low weight to aftershocks, the following weighting factor is applied:

$$w_i = \frac{\nu\lambda_0(t_i,m_i,x_i,y_i)}{\lambda'(t_i,m_i,x_i,y_i)}. \quad \text{(C11)}$$

[59] **Acknowledgments.** This work was supported by the International Science and Technology Fund administered by the Royal Society of New Zealand and the Institute of Geological and Nuclear Sciences. It also received support from the research project EPAN-M.4.3.6.1 funded by the General Secretariat of Research and Technology of Greece. Geophysics Department contribution 668. Frank Evison, supported by facilities provided under an honorary fellowship at Victoria University of Wellington, was the initiator of this collaborative study, but passed away before its completion. The authors are grateful to Joan Gomberg, Agnes Helmstetter, and an anonymous reviewer for their valuable comments and suggestions.

References

Aki, K. (1965), Maximum likelihood estimate of b in the formula log N = a − bM and its confidence limits, *Bull. Earthquake Res. Inst. Univ. Tokyo*, *43*, 237–238.

Aki, K. (1981), A probabilistic synthesis of precursory phenomena, in *Earthquake Prediction: An International Review*, *Maurice Ewing Ser.*, vol. 4, edited by D. W. Simpson and P. G. Richards, pp. 566–574, AGU, Washington, D. C.

Aki, K. (1989), Ideal probabilistic earthquake prediction, *Tectonophysics*, *169*, 197–198.

Chen, C.-C., J. B. Rundle, H. C. Li, J. R. Holliday, K. Z. Nanjo, D. L. Turcotte, and K. F. Tiampo (2006), From tornadoes to earthquakes: Forecast verification for binary events applied to the 1999 Chi-Chi, Taiwan, earthquake, *TAO*, in press.

Console, R. (2001), Testing earthquake forecast hypothesis, *Tectonophysics*, *338*, 261–268.

Console, R., and A. M. Lombardi (2002), Computer algorithms for testing earthquake forecasting hypotheses, *INGV Tech. Rep. 13*, Istituto Nazionale di Geofisica e Vulcanologia, Rome.

Console, R., and M. Murru (2001), A simple and testable model for earthquake clustering, *J. Geophys. Res.*, *106*, 8699–8711.

Console, R., M. Murru, and A. M. Lombardi (2003), Refining earthquake clustering models, *J. Geophys. Res.*, *108*(B10), 2468, doi:10.1029/2002JB002130.

Console, R., M. Murru, and F. Catalli (2006), Physical and stochastic models of earthquake clustering, *Tectonophysics*, *417*, 141–153.

Evison, F. F., and D. A. Rhoades (1997), The precursory earthquake swarm in New Zealand: Hypothesis test II, *N. Z. J. Geol. Geophys.*, *40*, 537–547.

Evison, F. F., and D. A. Rhoades (2001), Model of long-term seismogenesis, *Ann. Geofis.*, *44*, 81–93.

Evison, F. F., and D. A. Rhoades (2004), Demarcation and scaling of long-term seismogenesis, *Pure Appl. Geophys.*, *161*, 21–45.

Frankel, A. (1995), Mapping seismic hazard in the central and eastern United States, *Seismol. Res. Lett.*, *66*, 8–21.

Helmstetter, A., and D. Sornette (2002), Subcritical and supercritical regimes in epidemic models of earthquake aftershocks, *J. Geophys. Res.*, *107*(B10), 2237, doi:10.1029/2001JB001580.

Helmstetter, A., and D. Sornette (2003), Importance of direct and indirect triggered seismicity in the ETAS model of seismicity, *Geophys. Res. Lett.*, *30*(11), 1576, doi:10.1029/2003GL017670.

Helmstetter, A., G. Ouillon, and D. Sornette (2003), Are aftershocks of large Californian earthquakes diffusing?, *J. Geophys. Res.*, *108*(B10), 2483, doi:10.1029/2003JB002503.

Helmstetter, A., Y. Y. Kagan, and D. D. Jackson (2006), Comparison of short-term and time-independent earthquake forecast models for southern California, *Bull. Seismol. Soc. Am.*, *96*, 90–106.

Holliday, J. R., K. Z. Nanjo, K. F. Tiampo, J. B. Rundle, and D. L. Turcotte (2005), Earthquake forecasting and its verification, *Nonlinear Processes Geophys.*, *12*, 965–977.

Jackson, D. D., and Y. Y. Kagan (1999), Testable earthquake forecasts for 1999, *Seismol. Res. Lett.*, *70*, 393–403.

Kagan, Y. Y. (2002), Aftershock xone scaling, *Bull. Seismol. Soc. Am.*, *92*, 641–655, doi:10.1785/0120010172.

Kagan, Y. Y., and D. D. Jackson (2000), Probabilistic forecasting of earthquakes, *Geophys. J. Int.*, *143*, 438–453.

Keilis-Borok, V. I. (1990), The lithosphere of the Earth as a nonlinear system with implications for earthquake prediction, *Rev. Geophys.*, *28*, 19–34.

Keilis-Borok, V. I. (1996), Intermediate-term earthquake prediction, *Proc. Natl. Acad. Sci. U.S.A.*, *93*, 3748–3755.

Keilis-Borok, V. I., and V. G. Kossobokov (1987), Periods of high probability of occurrence of the world's strongest earthquakes, *Comput. Seismol.*, *19*, 45–53.

McKenzie, D. P. (1978), Active tectonics of the Alpine-Himalayan belt: The Aegean Sea and surrounding regions, *Geophys. J. R. Astron. Soc.*, *55*, 217–254.

Molchan, G. M. (1997), Earthquake prediction as a decision-making problem, *Pure Appl. Geophys.*, *149*, 233–247.

Ogata, Y. (1989), Statistical models for standard seismicity and detection of anomalies by residual analysis, *Tectonophysics*, *169*, 159–174.

Ogata, Y. (1998), Space-time point-process models for earthquake occurrences, *Ann. Inst. Stat. Math.*, *50*, 2, 379–402.

Papadimitriou, E. E., F. F. Evison, D. A. Rhoades, V. G. Karakostas, R. Console, and M. R. Murru (2006), Long-term seismogenesis in Greece: Comparison of the evolving stress field and precursory scale increase approaches, *J. Geophys. Res.*, *111*, B05318, doi:10.1029/2005JB003805.

Papazachos, B. C., and P. E. Comninakis (1970), Geophysical features of the Greek island arc and eastern Mediterranean ridge, *C. R. Seances Conf. Reunie Madrid, 1969*, *16*, 74–75.

Papazachos, B. C., P. E. Comninakis, G. F. Karakaisis, B. G. Karakostas, C. A. Papaioannou, C. B. Papazachos, and E. M. Scordilis (2005), A catalogue of earthquakes in Greece and surrounding area for the period 550BC–2005, Geophys. Dep., Thessaloniki Univ., Thessaloniki, Greece.

Papazachos, C. B., and A. A. Kiratzi (1996), A detailed study of the active crustal deformation in the Aegean and surrounding area, *Tectonophysics*, *253*, 129–153.

Reasenberg, P. A., and L. M. Jones (1989), Earthquake hazard after a main shock in California, *Science*, *243*, 1173–1176.

Rhoades, D. A., and F. F. Evison (1979), Long-range earthquake forecasting based on a single predictor, *Geophys. J. R. Astron. Soc.*, *59*, 43–56.

Rhoades, D. A., and F. F. Evison (1989), Time-variable factors in earthquake hazard, *Tectonophysics*, *167*, 201–210.

Rhoades, D. A., and F. F. Evison (2004), Long-range earthquake forecasting with every earthquake a precursor according to scale, *Pure Appl. Geophys.*, *161*, 47–72.

Rhoades, D. A., and F. F. Evison (2005), Test of the EEPAS forecasting model on the Japan earthquake catalogue, *Pure Appl. Geophys.*, *162*, 1271–1290.

Rhoades, D. A., and F. F. Evison (2006), The EEPAS forecasting model and the probability of moderate-to-large earthquakes in central Japan, *Tectonophysics*, *417*, 119–130.

Scordilis, E. M., G. F. Karakaisis, B. G. Karakostas, D. G. Panagiotopoulos, P. E. Comninakis, and B. C. Papazachos (1985), Evidence for transform faulting in the Ionian Sea: The Cephalonia Island earthquake sequence, *Pure Appl. Geophys.*, *123*, 388–397.

R. Console and M. Murru, Istituto Nazionale di Geofisica e Vulcanologia, Via Vigna Murata 605, I-00143 Rome, Italy. (console@ingv.it)

V. G. Karakostas and E. E. Papadimitriou, Geophysics Department, University of Thessaloniki, GR-54006 Thessaloniki, Greece.

D. A. Rhoades, Institute of Geological and Nuclear Sciences, 1 Fairway Drive, Lower Hutt 6009, New Zealand.